Range Image Techniques for Fast Detection and Quantification of Changes in Repeatedly Scanned Buildings

Zhizhong Kang, Liqiang Zhang, Huanyin Yue, and Roderik Lindenbergh

Abstract

This paper proposes a new method for the detection and quantification of changes in buildings using terrestrial laser scanning data from different epochs. A refined registration process is implemented that utilizes an optimized version of the Iterative Closest Point (ICP) algorithm, which implements the search of adjacent points in terms of their scanning angles. For detecting changes, a novel 2D angular difference histogram is proposed to first determine point segments representing building parts from the raw scattered scans. Afterwards, Hausdorff distance-based change detection is innovatively integrated into the optimized ICP process to improve the efficiency of the entire algorithm. The detected changes are quantified in the final step by determining the total planar surface area of the changed facade. This approach is tested and illustrated on two real datasets. The change quantification results show that the accuracy of the changed area quantification is in the order of square centimeters.

Introduction

The terrestrial laser scanning (TLS) point cloud provided by high-resolution laser scanners is both dense and accurate, thereby allowing the detection of small changes over time. Applications include the update of geographic information by comparing newly acquired information with the old state, the close-range safety monitoring during transportation, and control of building activities. Although much attention has been paid to large-scale change detection (e.g., Murakami *et al.*, 1999; Walter, 2004; Vögtle and Steinle, 2004; Matikainen *et al.*, 2004; De Chant and Kelly, 2009; Pollard *et al.*, 2010; Malinverni, 2011), the behavior of small-sized natural phenomena and the changes in specific objects are of great importance for the analysis of deformations or object evolution that require a more subtle analysis of the measured scene. Several deformation analysis approaches for designated objects have been discussed in recent years. An approach that employs terrestrial laser scanning data of a lock gate was presented by Schäfer *et al.* (2004). This method enabled deformation detection through the construction of a uniform and regular grid from each scattered point cloud. Instead of simple thresholding of differences, Lindenbergh and Pfeifer (2005) proposed a method to detect deformation below the nominal single point measurement accuracy using statistical deformation analysis based on the comparison of laser points and fitted planar segments between different epochs. Similarly, Kenner *et al.* (2011) presented a detailed spatial (by superficially extending the movement) and temporal (the number of epochs) analysis to detect changes smaller than the single point accuracy, which was applied in the monitoring of erosive processes in a rock wall. Gosliga *et al.* (2006) implemented deformation analysis on a bored tunnel by means of terrestrial laser scanning that included an analysis of both deformation between different epochs and deformations of the fitted tunnel with respect to the design model. Girardeau-Montaut *et al.* (2005) carried out a comparison study by using the Hausdorff distance as a measure for changes. They noted three issues to be addressed: point sampling variations between scans, computational costs of the Hausdorff distance, and real change discrimination. Zeibak and Filin (2007) also analyzed the potential artifacts that may affect the detection, which include resolution and object pose variations, occlusion and scanner-related artifacts (e.g., regions of no reflectance, range limitations, and noise). They proposed an approach for change detection through the use of TLS data in which the comparison is conducted through a mere image subtraction between the range images of a reference scan and the analyzed scan transformed into the reference frame to eliminate the artifacts mentioned above. As this method assumes that the transformation parameters are known, the reliability of image subtraction depends greatly on the registration accuracy between reference and analyzed scans.

In general, the challenges of change detection of buildings sampled by terrestrial laser scans comprise the irregular point distribution, the varying scale and resolution within the scene (depending on depth), the large data volume in each scan and falsely detected changes caused by factors such as the occlusion of objects or object parts, "no-reflectance" regions, range limits, noise, and errors in the registration

Zhizhong Kang is with the Department of Geodesy and Geomatics, School of Land Science and Technology, China University of Geosciences, Xueyuan Road 29, Haidian District, Beijing 100083, China (zzkang@cugb.edu.cn).

Liqiang Zhang is with the Research Center for Remote Sensing and GIS, School of Geography, Beijing Normal University, 100875 Beijing, China.

Huanyin Yue is with the National Remote Sensing Center of China, Ministry of Science and Technology, 100036 Beijing, China.

Roderik Lindenbergh is with the Chair Optical and Laser Remote Sensing, Dept. Geosciences and Remote Sensing, Faculty of Civil Engineering and Geosciences, Delft University of Technology, Stevinweg 1, 2628 CN, Delft, The Netherlands.

Photogrammetric Engineering & Remote Sensing
Vol. 79, No. 8, August 2013, pp. 000–000.

0099-1112/13/7908–0000/$3.00/0

To address those challenges, the present study, an extension of previous work (Kang *et al.*, 2010), proposes an efficient algorithm for detecting and quantifying changes in buildings applied on a time series of point clouds. The proposed method aims at detecting changes in the range of a few centimeters to meters. Therefore, these changes are above the signal to noise ratio of most scanners, which implies that there is no need for stochastic techniques which are powerful but less computational efficient. It should be applicable in those cases where 3D scan data can be organized in a so-called depth or range image format. This would make the method suitable for two common scan scenarios. First, the situation of repeated scans by a static terrestrial laser scanner, sampling the same building facades, and second, the situation of laser mobile mapping, In the first scenario, a depth or range image can be constructed by converting the 3D Cartesian coordinates in spherical coordinates, approximately centered at the scanner location; In the second scenario, Cartesian coordinates can be converted conveniently into cylindrical coordinates, where the cylinder axis corresponds to the car trajectory, and the two remaining cylindrical coordinates correspond to the perpendicular distance to the car trajectory and the vertical angle of the laser ray, respectively. However, this paper focuses on the first scenario.

The overall diagram of the proposed algorithm is illustrated in Figure 1. The automatic point cloud registration consists of determining point correspondences on panoramic reflectance images, correct correspondence identification using the RANSAC (RANdom SAmple Consensus; Fischler and Bolles, 1981) framework, optimal parameter computation through least-squares adjustment and registration refinement using an optimized ICP algorithm, which organizes 3D data in a 2D image format using the scanning angles of each laser point as indices. Building change detection first requires the generation of a 2D angular difference histogram to classify building point segments from the scattered point cloud for the purpose of discarding irrelevant points and thus significantly reducing the data volume involved in the process of change detection. Afterwards, a Hausdorff distance-based change detection is innovatively integrated into the refining registration process. After point-level change detection, the process of real change discrimination is implemented to exclude false changes. Finally, the changes are quantified by calculating the area of the region affected by change from a suitable TIN (Triangulated Irregular Network).

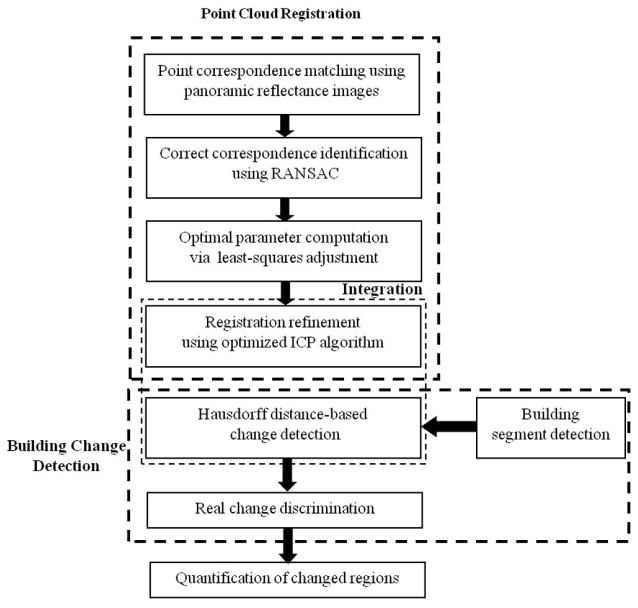

Figure 1. Diagram of the proposed method for the detection and quantification of changes in buildings.

We start by describing the automatic point cloud registration method using RANSAC and an optimized version of the ICP algorithm, which organizes 3D data in a 2D image format described in the next section, followed by the Hausdorff distance-based change detection algorithm. The next section presents the quantification of the changed regions from scattered point segments using planar surface area as the criterion, followed by a discussion of our test results, after which we offer our conclusions and suggestions for further research.

Automatic Point Cloud Registration

Because scan locations between epochs are in general not fixed, registration of two sets of epoch data is required before building change detection can be performed. We adopt our previous work, an approach for the automatic registration of terrestrial laser scanning (TLS) point clouds that uses panoramic reflectance images (Kang *et al.*, 2009) and optimize correct correspondence identification using the RANSAC framework, which eliminates the effect of outliers. Afterward, optimal transformation parameters are computed using least-squares adjustment. Furthermore, a refined registration process is implemented that utilizes an optimized ICP algorithm, by organizing 3D data in a 2D image format to enable rapid nearest neighbor search.

The method proposed by Kang *et al.* (2009) maps a 3D point cloud into a 2D reflectance image, which greatly simplifies the registration. The scale invariant feature transform (SIFT) method is utilized to make correspondence tracking feasible in the case of panoramic images. Using the corresponding points detected in the previous step, the transformation parameters between different coordinate frames are computed, resulting in the registration of the point clouds. In addition, the image point correspondence and the computation of the rigid transformation parameters (RTPs) are integrated into an iterative process that allows for further registration optimization.

RANSAC Framework

The objective of registration is to compute transformation parameters (i.e., nine elements of the rotation matrix and three elements of the translation vector) between different coordinate frames from 3D correspondences between two scans. The approach presented by Kang *et al.* (2009) employs least-squares adjustment for the absolute orientation in photogrammetry (Mikhail *et al.*, 2001) to solve for the least-squares optimized values of RTPs. However, this approach does not work when there are more than 50 percent outliers. RANSAC (RANdom SAmple Consensus; Fischler and Bolles, 1981) is therefore used to eliminate outliers first.

Rather than using as much of the data as possible to obtain an initial solution and then attempting to eliminate invalid data points, RANSAC tries many minimal random subsets and evaluate each subsets model fit. The RANSAC paradigm requires three parameters: (a) the error tolerance used to determine whether a point is compatible with a model, (b) the number of subsets to try, and (c) the number, *t*, of compatible points that is required for a model to be defined correct. The determination of these three parameters is discussed in the original RANSAC paper (Fischler and Bolles, 1981).

The 12 transformation parameters that comprise nine elements of the rotation matrix (instead of the three angles

to define a rotation) and three translation elements, are used because directly using the rotation matrix has good simplicity and compatibility both in the computation of RANSAC and the least squares optimization. Therefore, the number of scan points from which the model parameters are estimated is four, as at least four points are required to determine the twelve parameters of the rigid transformation between two scans.

To ensure the orthogonality of the calculated rotation matrix, we impose the following constraints on the computation (Equation 1):

$$\left.\begin{aligned} a_1^2+b_1^2+c_1^2&=1\\ a_2^2+b_2^2+c_2^2&=1\\ a_3^2+b_3^2+c_3^2&=1\\ a_1a_2+b_1b_2+c_1c_2&=0\\ a_1a_3+b_1b_3+c_1c_3&=0\\ a_3a_2+b_3b_2+c_3c_2&=0 \end{aligned}\right\} \quad (1)$$

where: $\begin{bmatrix} a_1 & a_2 & a_3\\ b_1 & b_2 & b_3\\ c_1 & c_2 & c_3 \end{bmatrix}$ denotes the rotation matrix.

The criterion of outlier identification is based on the evaluation of the geometric distances between the correspondence candidates after transformation. Using correct corresponding points, the optimal parameters are computed through least-squares adjustment.

Optimized ICP algorithm

Registration accuracy is of great importance for change detection. The Iterative Closest Point (ICP; Besl and McKay, 1992) algorithm is widely regarded as a good solution for achieving high registration accuracy; however, the efficiency of a nearest neighbor search over a large volume of data is a significant challenge that must be faced when using this search technique. Efficient variants of the ICP algorithm have been proposed to circumvent the exhaustive nearest neighbor search technique for the purpose of improving the efficiency of the algorithm (e.g., Godin and Boulanger, 1995; Sharp *et al.*, 2002).

Suppose that A_1 and A_2 are neighbors along the scanning direction. The Cartesian coordinate differences between their respective coordinates (X_1, Y_1, Z_1) and (X_2, Y_2, Z_2) may vary widely because A_1 and A_2 may be positioned at different ranges from the scanner. Thus, it is expected that it will be more difficult to determine a fast search in a Cartesian coordinate frame. However, in the spherical coordinate system, the differences between the angular coordinates (φ_1, θ_1) and (φ_2, θ_2) of A_1 and A_2 are independent of the corresponding range values. Moreover, according to the scanning mechanism of a terrestrial laser scanner, the neighborhood relationships of the consecutive laser rays, which can be derived from the corresponding scanning angles and angular resolutions, directly reflect those of the resulting laser points. Therefore, the search for adjacent points in terms of their scanning angles is expected to be free from the effects of irregular point distribution, varying scale and resolution within the scene (depending on depth) in 3D space, which makes the search simpler and faster.

For the TLS scans, the pre-defined angular resolution $\Delta\theta$ can be regarded as inherent parameter of the scan. Therefore, to further simplify the search process, the spherical coordinates are converted into a 2D coordinate system according to Equation 2 so that the nearest neighbor search can be implemented using 2D coordinates and the 2D coordinates can be used as the indices (row and column numbers of a 2D array) for the storage of the scattered point clouds:

$$\left.\begin{aligned} x&\frac{1}{\Delta\theta_H}\arctan\frac{Y}{X}\\ y&\frac{1}{\Delta\theta_V}\arctan\left(\frac{Z}{\sqrt{X^2+Y^2}}\right) \end{aligned}\right\} \quad (2)$$

where x and y are the 2D coordinates of a point; X, Y, and Z are the 3D coordinates from which the polar coordinates are derived; and $\Delta\theta_H$ and $\Delta\theta_V$ are the horizontal and vertical angular resolutions, respectively, of the scan.

Therefore, an efficient ICP algorithm that conducts this rapid nearest neighbor search is used to refine the registration results acquired by the approach presented above.

Figure 2 provides a visualization of the search process, in which we show the reflectance value of each laser point in the 2D coordinates computed using Equation 2. Figure 2a shows the 2D image of the reference scan in the pair-wise registration, Figure 2b is the reflectance image generated from the analyzed scan, while Figure 2c is formed by transforming the analyzed scan coordinates into the reference frame using the transformation parameters acquired by the approach presented above. Image 2c superposed on 2a with 70 percent opacity is presented in Figure 2d. The superposition shows that the nearest neighbor search can be narrowed down to a small range (e.g., 3 × 3 and 5 × 5) using the proposed rapid nearest neighbor search algorithm. This strategy is expected to remarkably reduce the complexity of a nearest neighbor search to O(N).

Building Change Detection

Forms of change can be primarily classified as deforming, disappearing, emerging, cracking, tilting/turning, and erosion. Relevant research has been conducted on deforming (e.g., Schäfer *et al.*, 2004; Lindenbergh and Pfeifer, 2005; Gosliga *et al.*, 2006) and emerging (e.g., Girardeau-Montaut *et al.*, 2005; Zeibak and Filin, 2007). In this paper, we focus on the change (a rigid body transformation, e.g., resulting from damage) detection of buildings and quantification of the changed regions, which can be helpful in applications such as disaster management and insurance claim evaluation.

The Hausdorff distance, or Hausdorff metric, measures how far two compact, non-empty subsets of a metric space are from each other, (Cain, 1994). The distance can be bidirectional or unidirectional. The latter distance is used herein and is a common distance that is used to compute, for each point p of a cloud S, the distance to the nearest point in the other cloud S':

$$d(p,S')=\min_{p'\in S'}\|p-p'\|_2 \quad (3)$$

In computer vision, the Hausdorff distance is used to find a given template in an arbitrary target image. Girardeau-Montaut *et al.* (2005) implemented a point-by-point comparison technique by using the Hausdorff distance as a measure of change and an octree as a data structure for accessing the 3D point cloud.

Integrated Registration and Change Detection Combining Optimized ICP Algorithm and Hausdorff Distance

The computational costs of the Hausdorff distance computation is a challenge that must be faced. If existing 3D building models are available, the change detection can be carried out by integrating these models with the scan data under analysis.

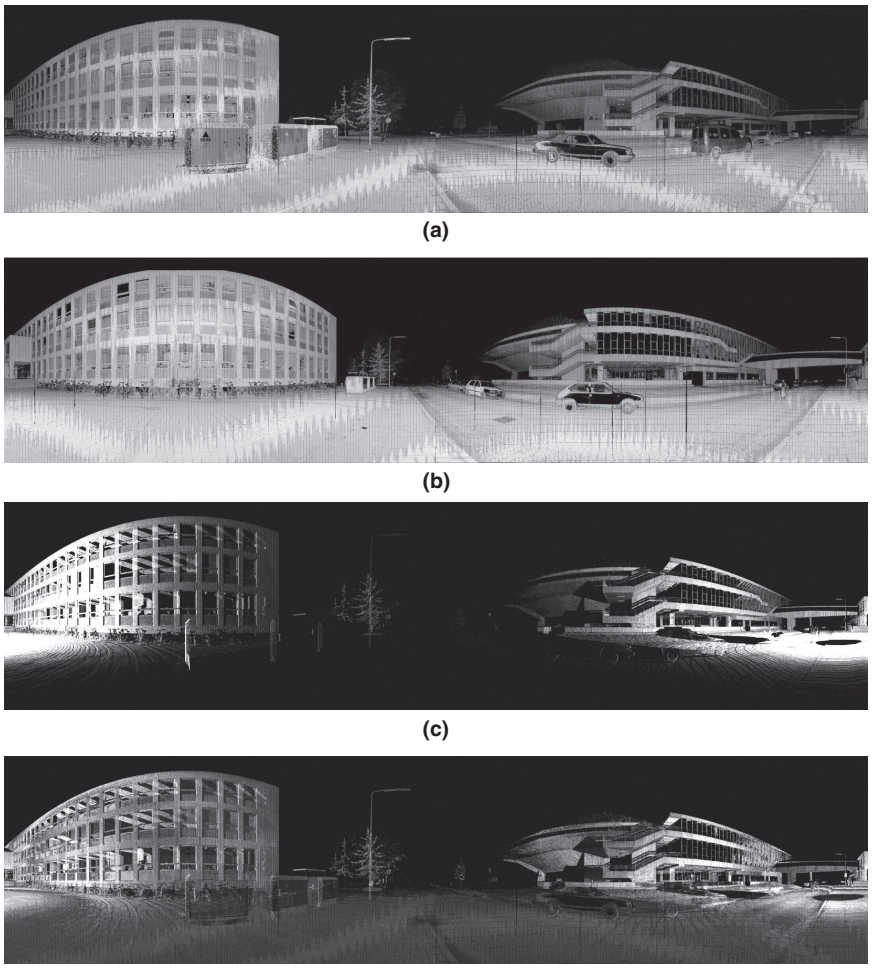

Figure 2. The organization of 3D data into a 2D image format: (a) the reflectance image generated from the reference scan, (b) the reflectance image generated from the analyzed scan, (c) the reflectance image of the analyzed scan transformed into the reference frame, and (d) the superposition of reflectance images.

In this context, we only need to implement the comparison using the Hausdorff distance for the point segments on each facet of the rebuilt building models. The computation time can be greatly shortened, as the search range is remarkably narrowed using this precondition.

As existing 3D building models are not always available, an algorithm that employs the Hausdorff distance but organizes 3D data in a 2D image format is proposed in this section with the purpose of reducing the computational costs of the Hausdorff distance computation. Moreover, Hausdorff distance-based change detection is integrated into the refining registration process using the optimized ICP algorithm presented in the previous section.

Zeibak and Filin (2007) implemented the comparison of scans through a mere image subtraction between the range images of the reference scan and analyzed scans transformed into the reference frame. However, the reliability of image subtraction greatly depends on the registration accuracy between the reference and analyzed scans. Because the ICP algorithm includes a nearest neighbor search in each iteration, change detection based on the Hausdorff distance can be integrated into the registration to improve the efficiency and to acquire a robust detection result.

The flowchart of the integration process is shown in Figure 3. Based on the generated reflectance images and computed RTPs, the reference and co-registrated scans of the 2D image are superimposed in the reference frame so that the rapid nearest neighbor search process presented in the previous section can be implemented to compute the unidirectional Hausdorff distance for each point of the compared scan. A threshold ε is set to identify a change. That is, if the computed unidirectional Hausdorff distance is larger than ε, the point is labeled as a change. Otherwise, it is added to the computation of the RTP update for the rapid nearest neighbor search of the 2D image in the next iteration. Iterations of change detection with the ICP continue until the maximum iteration limit is reached or the update becomes trivial.

Building Point Segment Classification

For the purpose of discarding irrelevant points, and thus, to significantly reduce the data volume involved in the process

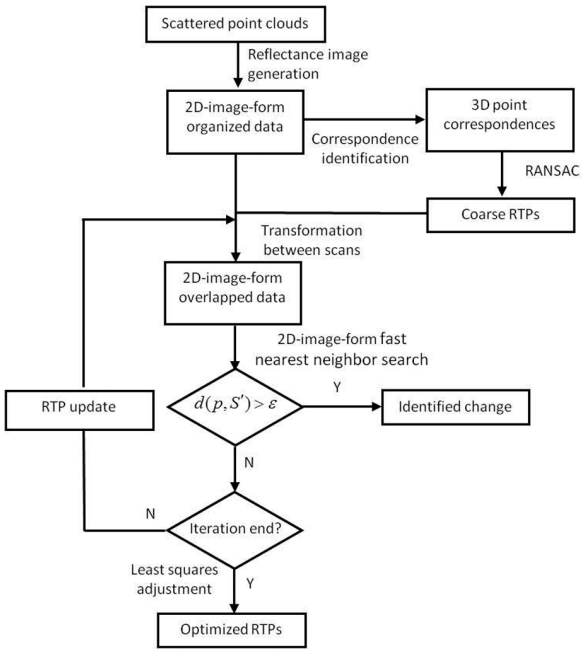

Figure 3. A flowchart of the change detection and registration integration process.

of change detection, in this section, building point segments are classified from TLS scans using a 2D angular difference histogram.

Frueh *et al.* (2005) proposed a strategy to detect the main building facade usiong a 2D histogram of the depth information in scans, which was based on the assumption that building facades were roughly perpendicular to the driving direction. This assumption fails to be valid in general because the TLS instrument pivots on a fixed plumb axis during scanning. As previously mentioned, according to the scanning mechanism of the terrestrial laser scanner, the neighborhood relationships of scanning laser rays directly reflect those of the resulting laser points. Figure 2a shows that neighboring points on a building or the ground usually have similar horizontal and vertical angles. Moreover, it also illustrates that such points are in the majority in the point cloud. The points on the ground can be filtered out using their *z* coordinate because a ground point has a relatively small *z* value, and its neighbors in the same scan column have a similarly low *z* value. Therefore, we generate a 2D angular difference histogram for building point segment classification as follows.

The histogram takes one scan organized as range (depth) image as input, that is, each 3D scan point is parameterized by a horizontal scan angle, a vertical scan angle, and a range distance. In the range image, the horizontal and vertical axes correspond to the horizontal and vertical scan angles, respectively. Now the range image is divided into cells of 1 × 1 degree. So, a full panoramic scan would consist of 360 × 360 cells. For each point in a given cell, the minimal difference in range (depth) between that point and the ranges of the other points in the cell is determined. If this minimum is below a given threshold, the point will be counted for the number of histogram points in the cell considered. That is, in the histogram, the horizontal, vertical, and upright axes denote the horizontal angle, vertical angle, and the number of points belonging to a grid cell, respectively, as shown in Figure 4. The grayscale legend shows that the gray scale varies from black to white, which represents increasing numbers of points per grid cell. Both the height and gray value of a rectangle denote, within a 1 degree × 1 degree grid cell, the number of points whose angular differences from their neighboring points are smaller than a chosen threshold. Figure 4 shows that the building segments have large and continuous distributions of rectangles. As a result, building detection can be performed by recognizing such patterns.

To facilitate the process of building detection, the 2D angular difference histogram is converted into a gray-scale image where gray values are scaled in terms of the rectangle height and where isolated outliers are removed by applying a median filter (Figure 5). An image segmentation method using graph theory (Felzenszwalb and Huttenlocher, 2004) is utilized to abstract the building segments from the gray-scale image. Figure 6a shows the results of the segmentation of the angular difference histogram. Among the segmented patches, the patches on the building, indicated by white arrows, always occupy dominant areas in the image. Therefore, we aggregate these patches into building point segments

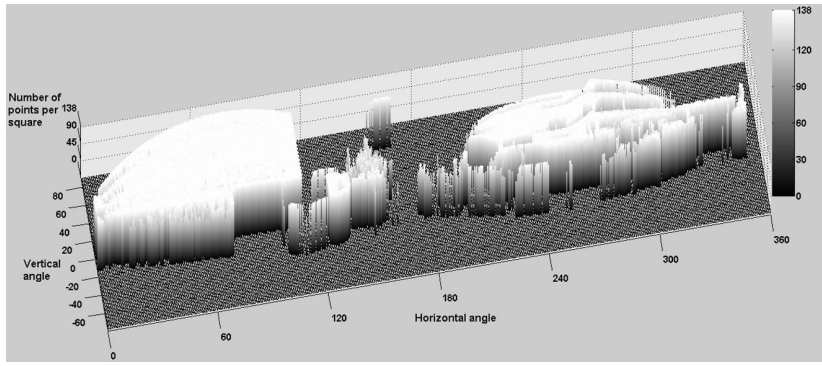

Figure 4. Two-dimensional angular difference histogram: the horizontal, vertical, and upright axes denote the horizontal angle, vertical angle, and the number of points belonging to a grid cell, respectively.

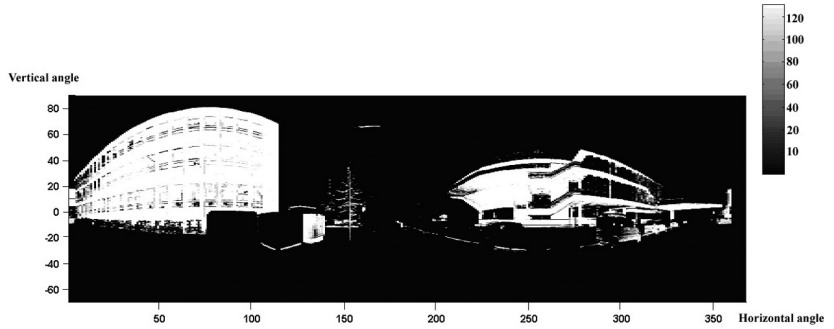

Figure 5. The angular difference histogram as a gray-scale image.

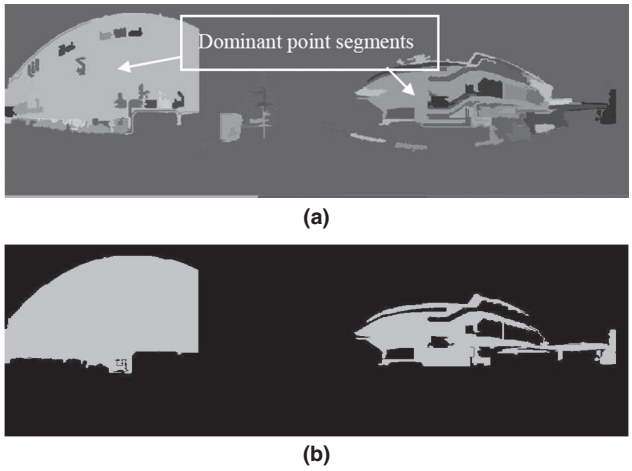

Figure 6. Building point segment classification: (a) segmentation resulting from analyzing the angular difference histogram, and (b) building point segments remaining after discarding isolated and empty segments.

(Figure 6b) by merging their conterminous segments and discarding empty ones (no laser point inside). The change detection process is only implemented on the classified building point segments for the purpose of reducing data volume and, consequently, computation cost.

Identifying Real Change

After the building segmentation step, as described in the previous section, we assume at this stage that we have at least two segmented scans, i.e., one for each epoch. All isolated and/or noisy points have been removed in the previous step as not belonging to any segment. In this paragraph it is described how real changes are distinguished from occlusions.

Occlusion of object parts may occur when the scanning position changes. Figure 7 shows a portion of a scene in 3D space (highlighted in a chess pattern), which is observed in one scan but is missing in the other scan due to occlusion. Those points appearing in one scan but not in the other are natural change candidates, which may lead to false detections. To address occlusion effects, Girardeau-Montaut *et al.* (2005) utilized the depth image generated from the scan, which is equivalent to a *Z*-buffer (Watkins, 1970). The reflectance image used in the registration stage is similar

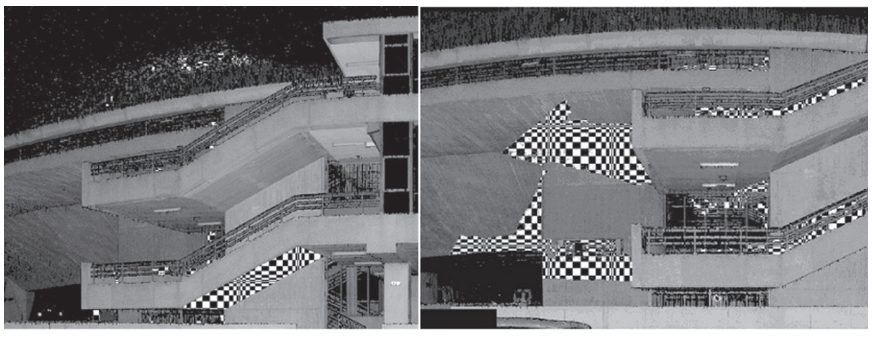

Figure 7. Occlusions due to a change in scanning position which is (a) observed in one scan but is (b) missing in the other scan due to occlusion.

to the depth image; thus, it can easily be converted to the depth image by simply replacing the reflectance value with the range. With regard to the detection of both disappearing and emerging changes, we first generate the range images of a reference scan, and then transform the analyzed scan into the reference frame. The range values between overlaying pixels in the building segments are then compared. As a result, the points in the analyzed range image with larger range values that are highlighted in the chess patterns (Figure 7) are considered unchanged because they are occluded.

Quantification of Changed Regions

Because the results of change detection using the Hausdorff distance consist of a number of scattered points (Figure 8a), one needs to quantify the changed regions before the results can be applied for, e.g., disaster management or insurance claim evaluation. The volume of the changed region is certainly an optimal criterion of quantification if an accurate 3D model is available. However, often assumptions are necessary on occluded and incompletely scanned areas when a watertight 3D model is constructed from scan data, which may lead to a larger approximation errors. Therefore, instead of volume, we chose the planar surface area of the changed part of the building facade as the criterion of quantification in this context.

As in our previous work, the approach proposed by Xu *et al.* (2009) is employed to implement segmentation on each point segment marked as changed (Figure 8a). Based on the reflectance image generated from the point cloud, this method integrates image segmentation using graph theory (Felzenszwalb and Huttenlocher, 2004) with point cloud segmentation using region growing. Planar surfaces are then extracted (Figure 8b). To compute their areas, we generate a TIN (Triangulated Irregular Network) for each point segment that is marked as changed (Figure 8c) and compute the area of the entire changed region by summing the area of each triangle.

Due to a lack of proximity between vertices, the generated TIN comprises many triangles that appear along the outer boundary (wall outline) or within the inner boundaries (holes) of a wall, which should not be included in the area computation (Figure 8c). Therefore, the triangles whose edges are longer than a certain threshold, which is determined in terms of the sampling interval of the scan, are removed from the generated TIN that is used in the surface area calculation. Figure 8d illustrates that the remaining TIN mesh accurately describes the distribution of the point segment in Figure 8a. Next, the planar surface area is computed using Equation 4, which is derived from Heron's Formula (Cain, 1994). If the changed region is distributed across more than one planar facet, the planar surface area of the changed region is calculated by summing the Δ_{CR} of each facet:

$$\Delta_{CR} = \sum_{i=1}^{n} \sqrt{s_i (s_i - a_i)(s_i - b_i)(s_i - c_i)} \tag{4}$$

where Δ_{CR} = the area of the changed region, n = the number of triangles of the TIN mesh, a_i, b_i, c_i = the lengths of the sides of triangle I, s_i = the semiperimeter of triangle I, and s_i is computed as follows:

$$s_i = \frac{1}{2}(a_i + b_i + c_i). \tag{5}$$

The accurately computed surface areas can be used as a convincing baseline with which to estimate the damage or erosion of a building facade to evaluate an insurance claim, e.g., damage rate R_D of a building as calculated using Equation 6:

$$R_D = \frac{\Delta_{CR}}{\Delta_{OR}} \tag{6}$$

where Δ_{OR} and Δ_{CR} denote the areas of the original and changed regions, respectively.

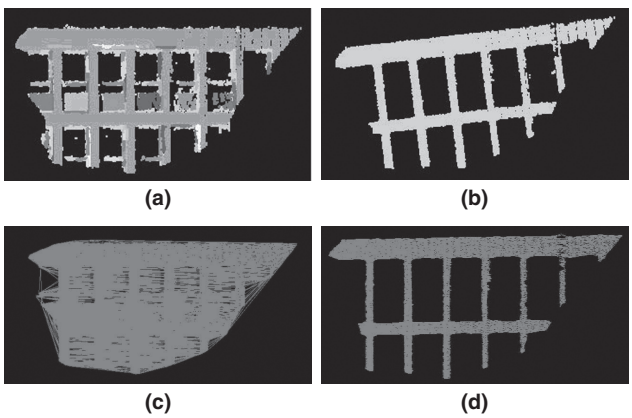

Figure 8. Quantification of the changed region: (a) the detected point segment, (b) the extracted planar segment, (c) the generated TIN mesh, and (d) the refined TIN mesh.

Experimental Results

The proposed approach was tested on two datasets acquired by the FARO LS 880 and RIEGL LMS-Z620 laser scanners, respectively. Table 1 describes the test point clouds. Dataset 1 (33 million laser points) contains two FARO TLS point clouds sampling the Aula Conference Centre of TU Delft (Delft University of Technology), The Netherlands, while Dataset 2 (10 million laser points) comprises two epochs of RIEGL point clouds, obtained over a two-week interval, corresponding to the construction of a simple building on the campus of Capital Normal University in Beijing, China.

Automatic Registration of TLS Point Clouds

The registration method proposed in the *Automatic Point Cloud Registration Section* was tested on both data sets.

Performance Comparison between the RANSAC Framework and Least Squares Adjustment

The performance of the method enhanced by RANSAC, and the least squares adjustment were compared using synthetic data in terms of deviations from the designed RTPs. Figure 9 shows the distribution of the 589 laser points chosen from the

Table 1. Description of the Test Point Clouds

Point cloud	Scan Angular resolution	Range accuracy
Datasets 1	0.036°/0.036°	±3 mm
Datasets 2	0.046°/0.046°	±10 mm

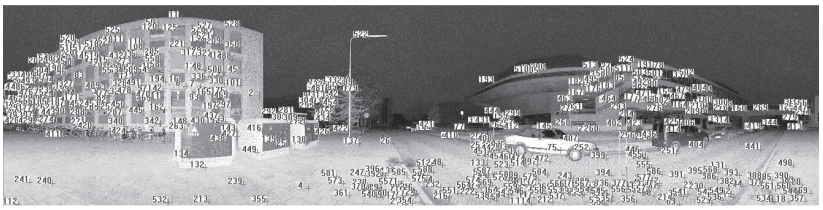

Figure 9. The laser points chosen from FARO_LS_007.

FARO_LS_007 scan of Dataset 1. They were transformed into a synthetic point cloud with the designed RTPs shown below.

$$R = \begin{bmatrix} 0.99985696 & -0.01691026 & -0.00032523 \\ 0.01691035 & 0.99985697 & 0.00027301 \\ 0.00032057 & -0.00027847 & 0.99999991 \end{bmatrix}$$

$$T = \begin{pmatrix} -12.22282391 & -2.85676022 & 0.01788418 \end{pmatrix}.$$

We assigned a random error of within one centimeter to 3D coordinates and a gross error reaching 10 centimeters to a certain number of coordinates. Table 2 lists the performance of RANSAC and the least squares adjustment against different percentages of outliers. As Table 2 shows, as far as the least-squares adjustment is concerned, the RMS error and deviations from the designed RTPs are small when the outlier percentage is within 30 percent; however, they become unacceptable once the outlier percentage increases, which shows that least squares adjustment does not work when the outlier percentage is more than 30 percent. In contrast, RANSAC achieved robust results over a wide range (between 10 and 80 percent) of outlier percentages. These results prove that RANSAC performs well in correct correspondence identification and optimal parameter computation against outliers.

Optimized ICP Algorithm Results

The registration process previously presented utilizing an optimized ICP algorithm that organizes 3D data using the scanning angles of each laser point as indices was tested on Dataset 1 and compared with an efficient ICP algorithm that uses the K-D tree search algorithm, because it is one of the most effective algorithms with which to establish the closest point relationships with a complexity of O(NlogN). Two search ranges, i.e., 3 × 3 and 5 × 5, were employed in the presented algorithm for experimental purposes. The registration results are listed in Table 3, and show that the accuracies of the three strategies are of the same order of millimeters; however, the computation time of a single nearest neighbor search process of the proposed algorithm significantly decreases compared with that of the ICP algorithm using the K-D tree. Because RANSAC ensured a robust correct correspondence identification against outliers, the computed parameters narrowed the nearest neighbor search to a very small range. As a result, the registration accuracies of the proposed approach using either a 3 × 3 or a 5 × 5 search range do not differ greatly.

Building Change Detection Results

To verify the building change algorithm as proposed in the *Building Change Detection Section* both synthetic and real data was tested.

Synthetic Changes in Dataset 1

We focus in this paper on detecting regular changes (rigid body transformations, due to, e.g. emerging, damaging, demolishing, etc.) of buildings. However, even though we could find a demolishing site, we failed to acquire data because of safety concerns. Therefore, we removed five parts from the

Table 2. Performance Comparison between Least-Squares Adjustment and RANSAC against Different Outlier Percentages: L Denotes Least-Squares Adjustment and R represents RANSAC

Outlier percentage	RMS (m)	$\Delta\phi$ (deg.)	$\Delta\omega$ (deg.)	Δk (deg.)	ΔX (m)	ΔY (m)	ΔZ (m)
10% (L)	0.002873	0.002241	0.001467	0.000312	0.000098	0.000040	0.000152
10% (R)	0.002880	0.000312	0.000030	0.000331	0.000017	0.000027	0.000020
20% (L)	0.002846	0.000992	0.000415	0.000259	0.000018	0.000070	0.000046
20% (R)	0.002894	0.000284	0.001332	0.000067	0.000118	0.000060	0.000192
30% (L)	0.002864	0.003733	0.005041	0.000120	0.000165	0.000301	0.000102
30% (R)	0.002844	0.002047	0.002006	0.000938	0.000033	0.000194	0.000062
40% (L)	0.914939	0.463286	0.734808	0.348716	0.071901	0.057348	0.020988
40% (R)	0.002900	0.000671	0.000376	0.000374	0.000087	0.000047	0.000555
50% (L)	0.995497	0.073870	0.372337	0.124763	0.012890	0.026332	0.082774
50% (R)	0.002818	0.000295	0.000366	0.000128	0.000008	0.000182	0.000076
80% (L)	1.330843	1.029302	0.176333	0.099592	0.054077	0.032687	0.059979
80% (R)	0.002856	0.001535	0.001294	0.000372	0.000072	0.000455	0.000436

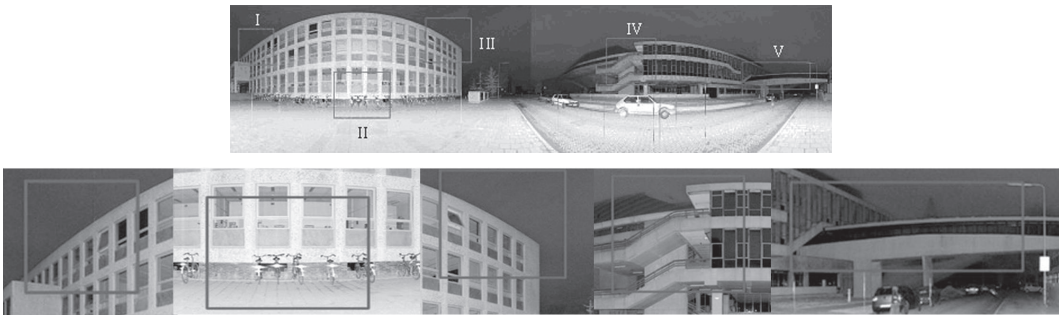

Figure 10. Synthetically changed regions.

TABLE 3. RESULTS OF REGISTRATION

Method	RMS (m)	Computation time of a single nearest neighbor search process (s)
ICP using K-D tree	0.001628	135
Proposed method (5 × 5)	0.001953	43
Proposed method (3 × 3)	0.001959	26

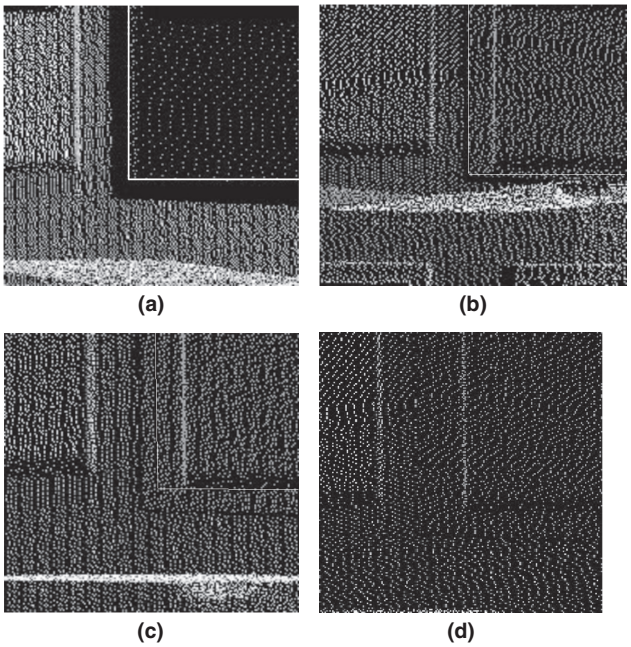

Figure 11. The detected boundaries using different search ranges: the cracks between the detected (highlighted by the white lines) and synthetic boundaries become smaller when the search range varies from 4 × 4 to 20 × 20: (a) 4 × 4, (b) 10 × 10, (c) 16 × 16, and (d) 20 × 20.

FARO_LS_009 scan of Dataset 1 to simulate disappearance due to damage or demolishment (Figure 10). Then, the data with and without the five parts were compared using the method of the *Building Change Detection Section*.

As illustrated in Figure 11, experiments were performed to detect the synthetic changes using four different search ranges, varying from 4 × 4 to 20 × 20. The results (e.g., region III in Figure 10) show that the cracks between the detected (highlighted by the white lines) and synthetic boundaries become smaller with increasing search range. The range of 20 × 20 ensured an optimal approximation of the synthetic boundary of the changed region because the accumulation of registration error and resolution differences between point clouds scanned at different positions, led to a large search area.

After applying the building segment detection and real change discrimination techniques previously proposed, the changed regions detected from Dataset 1 were obtained as illustrated in Figure 12.

As shown in Figure 12a, the dark regions were identified as changes. In addition to the synthetic region, the points within the white box on the left belong to an open window that was closed during the data acquisition and thus

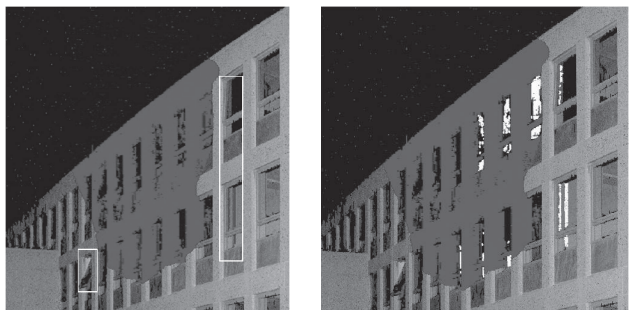

Figure 12. Real change discrimination results: the dark regions were identified as changes: (a) before occlusion detection, and (b) after occlusion detection.

correspond to real change. However, the dark parts in the right rectangle were falsely detected, as they were located on the wall in a room that became occluded during the scanning. Figure 12b illustrates that the occluded parts (highlighted in white) were detected using the occlusion detection algorithm previously presented. They were removed from the list of detected regions of change.

Real Changes due to Construction Work in Dataset 2

Although the TLS in general does not hit the same object points at two different epochs, it is reasonable to assume that the deviation will not exceed the sampling interval of the scan. A modern scanner is capable of acquiring data with very high spatial resolution. As far as the RIEGL LMS-Z620 scanner is concerned, its highest angular resolution is 0.002 deg. The resolution of the RIEGL dataset was set as 0.046 degrees. Therefore, the deviation is expected to be smaller than the spatial sampling interval of 8 mm at a 10 m distance from the origin of the scanner, which is acceptable for our proposed algorithms. This resulting point density was also considered in setting the threshold ε for identifying changes.

Figure 13 shows the real changes as sampled by the scans from both epochs. These changes are due to the construction work between the two acquisitions. Each epoch contains two point clouds that were acquired from two different locations. During the two weeks between scanning, the building site changed remarkably, e.g., a simple building was constructed, the brick pile was used up, falsework was removed, and new accumulations of building material were placed on the site.

The results of the change detection at the construction site using the Hausdorff distance, comparing the *Building Change Detection Subsection*, are shown in Figure 13c. A comparison to Figure 13a and 13b shows that visual recognizable changes were indeed automatically detected by the Hausdorff method. Additionally, tree branches and leaves were regarded as changes by the automatic method because they were moving during the scanning process. By comparing Figure 13a with 13b, it can be observed that the exterior walls of the simple building in 13a had been coated. Figure 14 shows the detected additive coating of the wall. Although the scanned surfaces of the exterior walls in different epochs are non-superimposed layers because of the additive coating, the average distance between them is only approximately 1 cm. As we did not focus on subtle changes in this study, the exterior wall coating was omitted from the list of detected changes.

The change in the façade of the simple building is illustrated in Figure 15. The light segment represents the unfinished façade, while the dark segment denotes the completed façade. Superimposing both segments shows that the detected boundary perfectly matches the upper outline of the uncompleted facade.

Figure 16a also shows that some parts of the facade were occluded by the falsework in front of it, during the scanning process. As Figure 15 shows, those regions were detected

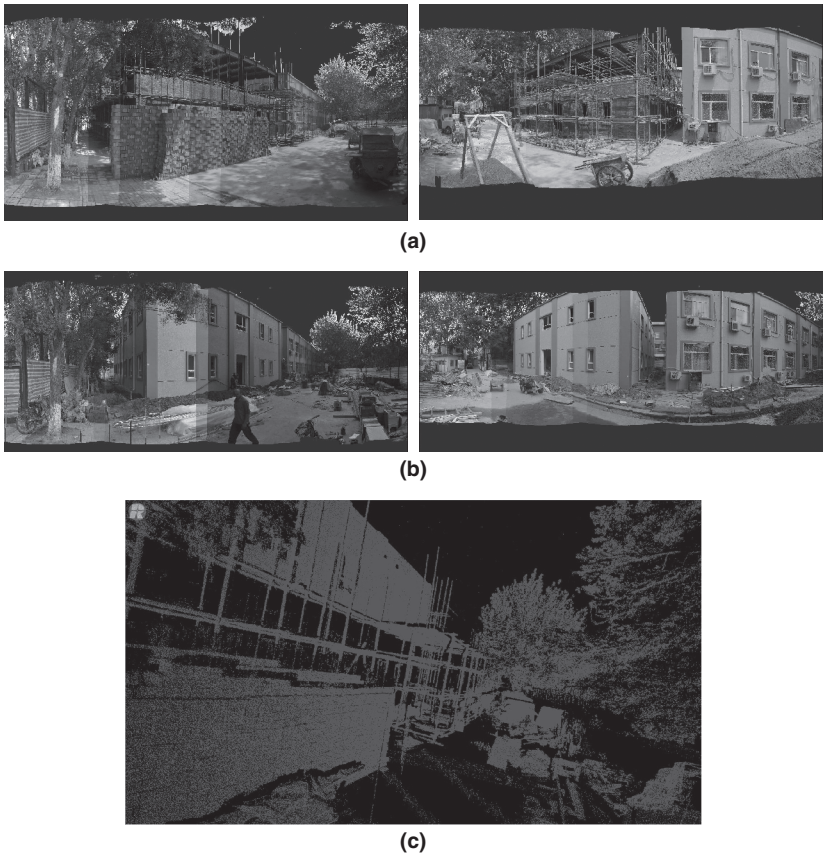

Figure 13. Real change captured during a two-week time period: (a) the construction site recorded in Epoch I, (b) the construction site recorded in Epoch II, and (c) changes detected at the construction site.

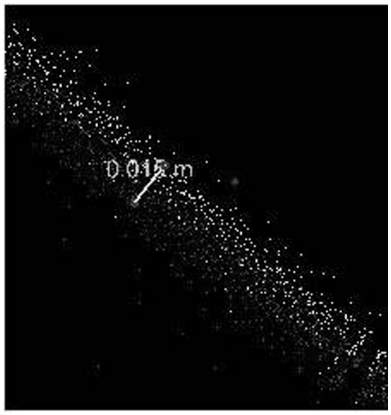

Figure 14. The detected additive coating of the wall.

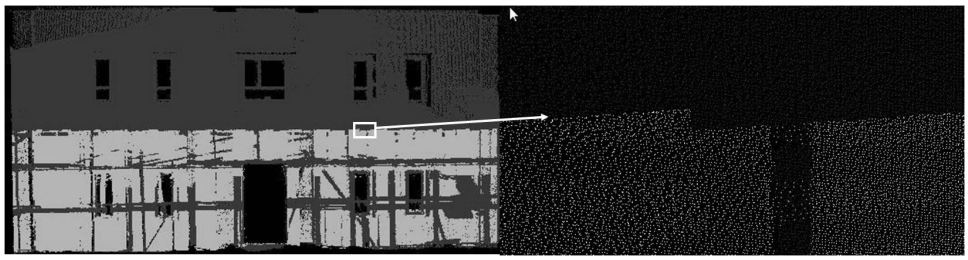

Figure 15. The detected change in the façade of the simple building.

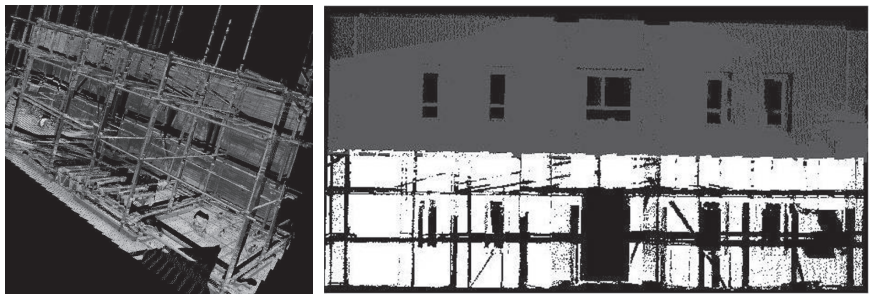

(a) (b)

Figure 16. The detected real changes in Dataset 2: the dark regions were identified as changes: (a) the occlusion of falsework, and (b) detected real change.

as areas of change and were later removed through the real change discrimination process; compare the *Identifying Real Change Subsection* (Figure 16b).

Quantification of Changed Regions

In this paragraph the methods of the *Identifying Real Change Subsection* are applied to quantify the found changes, that is, a TIN mesh of the changed area is created in which long edges are removed. Figure 17 illustrates that the refined TIN meshes accurately describe the distribution of the point segments in Figure 16.

The planar surface area was computed using Equation 4. Table 4 shows the quantification results. To verify the quantification accuracy, we need to have known reference data. Concerning Dataset 1, we evaluated the change quantification accuracy by comparing the quantification results with the areas of the synthetic regions. The RMS error of the quantification of the detected synthetic changes is 0.0049 m^2. This accuracy is expected to meet the needs associated with, for example, disaster management and insurance claim evaluation.

As far as Dataset 2 is concerned, it is difficult to acquire reference data on a wall during actual building activities. The detected boundaries were therefore visually evaluated, by illustrating the detected change regions and unchanged parts with big grey contrast (Figure 15 and Figure 17(b)).

Conclusions

In this paper, we have proposed an algorithm for identifying and quantifying changes in buildings that uses a series of point cloud epochs as input and that consists of three steps: (a) automatic point cloud registration utilizing the RANSAC framework and an optimized ICP algorithm that organizes 3D data into a 2D image format, (b) ICP and Hausdorff distance-based change detection integration, and (c) quantification of changed regions.

The proposed algorithm was implemented using TLS data. The results of point cloud registration show that, because the RANSAC framework can ensure robust, correct correspondence identification against outliers, the computed parameters strongly narrow the nearest neighbor search. As a result, the computation time of a single nearest neighbor search of the proposed algorithm decreases remarkably compared with that of the ICP algorithm using the K-D tree algorithm. The results of the proposed change detection algorithm indicate that the Hausdorff distance is a good metric for change detection. The results also show that the changed regions can be accurately described through the construction of a TIN from the scattered points and exclusion of the holes and irrelevant triangles along the outer boundary. The quantification results show that, compared with the planar areas of the synthetic regions, the RMS error of the detected change quantification is expected to meet the needs associated with, for example, disaster management and insurance claim evaluation.

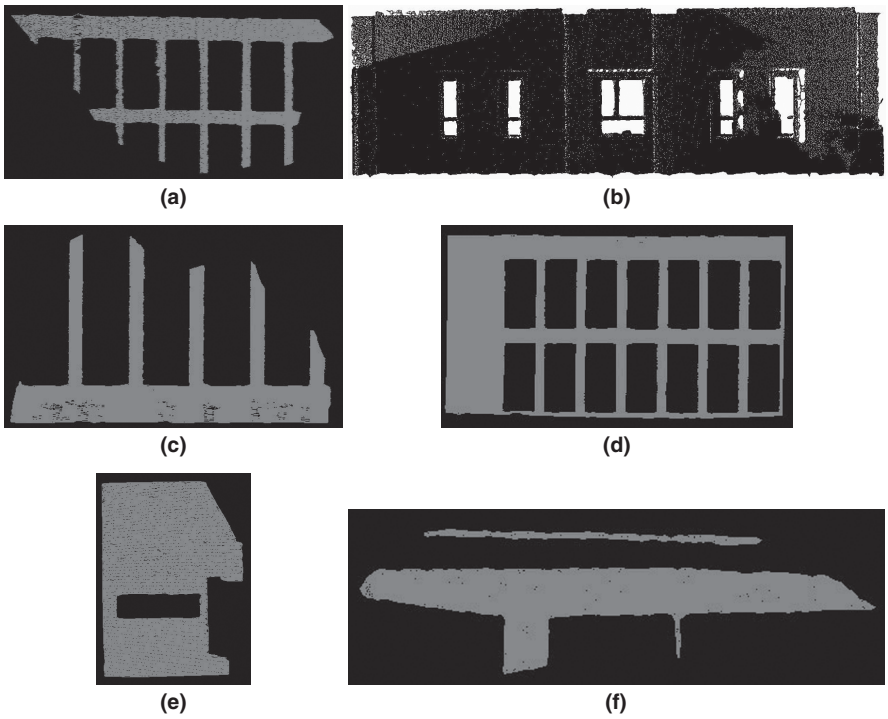

Figure 17. Refined TIN meshes: (a) Region I, (b) the façade of the simply constructed building, (c) Region II, (d) Region III, (e) Region IV, and (f) Region V.

TABLE 4. RESULTS OF CHANGE QUANTIFICATION

Detected Region	Area of synthetic region (m2)	Area of detected region (m2)	Δ (m2)
I	72.6622	72.6562	0.0060
II	62.6486	62.6452	0.0034
III	120.6387	120.6355	0.0032
IV	296.3596	296.3543	0.0053
V	95.8268	95.8208	0.0060
Constructing facade	×	45.4934	×

Future work will concentrate on the change quantification of complex surfaces and bodies, as well as the adaption of the proposed algorithm to change detection using mobile laser scanning data. In addition, it should be considered how the proposed methodology should be adapted to also retrieve volumetric changes instead of just quantifying the total area on a facade that has changed.

Acknowledgments

The comments of anonymous reviewers for improvement of this paper are gratefully acknowledged. This research was supported by the Natural Science Foundation of China under Grant No. 41171358 and the Fundamental Research Funds for the Central Universities.

References

Besl, P.J., and N.D. McKay, 1992. A method for registration of 3-D shapes, *IEEE Transactions on Pattern Analysis and Machine Intelligence*, 14(2):239–256.

Cain, G.L., 1994. *Introduction to General Topology*, Addison-Wesley.

De Chant, T., and M. Kelly, 2009. Individual object change detection for monitoring the impact of a forest pathogen on a hardwood forest, *Photogrammetric Engineering & Remote Sensing*, 75(8):1005–1013.

Felzenszwalb, P.F., and D.P. Huttenlocher, 2004. Efficient graph-based image segmentation, *International Journal of Computer Vision*, 59(2):167–181.

Fischler, M.A., and R.C. Bolles, 1981. Random sample consensus: A paradigm for model fitting with applications to image analysis and automated cartography, *Communications of the ACM*, 24:381–395, doi:10.1145/358669.358692.

Frueh C., S. Jain, and A. Zakhor, 2005. Data processing algorithms for generating textured 3D building facade meshes from laser scans and camera images, *International Journal of Computer Vision*, 61(2):159–184.

Girardeau-Montaut, D., M. Roux, R. Marc, and G. Thibault, G., 2005. Change detection on points cloud data acquired with a ground laser scanner, *International Archives of Photogrammetry, Remote Sensing*, 36(3/W19):30–35.

Godin, G., and P. Boulanger, 1995. Range image registration through viewpoint invariant computation of curvature, *International Archives of Photogrammetry and Remote Sensing*, Zurich, Switzerland, 30(5/W1):170–175.

Gosliga, van R., R. Lindenbergh, and N. Pfeifer, 2006. Deformation analysis of a bored tunnel by means of terrestrial laser scanning, *International Archives of Photogrammetry, Remote Sensing and Spatial Information Science*, 36(5):167–172.

Kang, Z., J. Li, L. Zhang, and S. Zlatanova, 2009. Automatic registration of terrestrial point clouds using reflectance panoramic images, *Sensors*, 9, doi: 10.3390/sensors.

Kang, Z., and Z. Lu, 2010. The change detection of building models using epochs of terrestrial point clouds, *International Archives of the Photogrammetry, Remote Sensing and Spatial Information Science*, Kyoto Japan, 38(8):231–236.

Kenner, R., M. Phillips, C. Denier, P. Thee, and A. Zgraggen, 2011. Investigation of rock and ice loss in a recently deglaciated mountain rock wall using terrestrial laser scanning: Gemsstock, Swiss Alps, *Cold Regions Science and Technology*, 67(3):157–164.

Lindenbergh, R., and N. Pfeifer, 2005. A statistical deformation analysis of two epochs of terrestrial laser data of a Lock, *Proceedings of the 7th Conference on Optical 3-D Measurement Techniques* (A. Gruen and H. Kahmen, editors), 03-05 October, Vienna, Austria, Vol. II, pp. 61–70.

Malinverni, E.S., 2011. Change detection applying landscape metrics on high remote sensing images, *Photogrammetric Engineering & Remote Sensing*, 77(10):1045–1056.

Matikainen, L., J. Hyyppä, and H. Kaartinen, 2004. Automatic detection of changes from laser scanner and aerial image data for updating building maps, *International Archives of the Photogrammetry, Remote Sensing and Spatial Information Sciences*, Istanbul, Turkey, 35(B2):434–439.

Mikhail, E.M., J.S. Bethel, and J.C. McGlone, 2001. *Introduction to Modern Photogrammetry*, John Wiley, New York, 496 p.

Murakami, H., K. Nakagawa, H. Hasegawa, I. Shibata, and E, Iwanami, 1999. Change detection of buildings using an airborne laser scanner, *ISPRS Journal of Photogrammetry and Remote Sensing*, 54(2-3):148–152.

Pollard, T.B., I. Eden, J.L. Mundy, and D.B. Cooper, 2010. A volumetric approach to change detection in satellite images, *Photogrammetric Engineering & Remote Sensing*, 76(7):817–831.

Schäfer, T., T. Weber, P. Kyrinovič, and M. Zámečniková, 2004. Deformation measurement using terrestrial laser scanning at the hydropower station of Gabčíkovo, *Proceedings of INGEO 2004 and FIG Regional Central and Eastern European Conference on Engineering Surveying.*, 11-13 November, Bratislava, Slovakia, unpaginated CD-ROM.

Sharp, G.C., S.W. Lee, and D.K. Wehe, 2002. ICP registration using invariant features, *IEEE Transactions on Pattern Analysis and Machine Intelligence*, 24(1):90–102.

Vögtle, T., and E. Steinle, 2004. Detection and recognition of changes in buildings geometry derived from multitemporal laserscanning data, *International Archives of Photogrammetry and Remote Sensing*, 35(B3), unpaginated CD-ROM.

Watkins, G.S., 1970. *A Real-time Visible Surface Algorithm*, Technical Report UTEC-CSc-70-101, Department of Computer Science, University of Utah, Salt Lake City, Utah.

Walter, V., 2004. Object-based classification of remote sensing data for change detection, *ISPRS Journal of Photogrammetry and Remote Sensing*, 58(3-4):225–238.

Xu, W., Z. Kang, and T. Jiang, 2009. A segmentation approach for terrestrial point clouds based on the integration of graph theory and region growing, *Proceedings of 2009 Urban Remote Sensing Joint Event*, 20-22 May, Shanghai, China, unpaginated CD-ROM.

Zeibak, R., and S. Filin, 2007. Change detection via terrestrial laser scanning, *International Archives of Photogrammetry and Remote Sensing*, 36(3/W52):430–435.

(Received 27 January 2012; accepted 22 March 2013; final version 26 March 2013)